Iron-mediated anaerobic ammonium oxidation recorded in the early Archean ferruginous ocean

Alice Pellerin, Christophe Thomazo, Magali Ader, Johanna Marin-carbonne, Julien Alleon, Emmanuelle Vennin, Axel Hofmann

Received: 20 June 2022 | Revised: 17 November 2022 | Accepted: 3 December 2022

DOI: 10.1111/gbi.12540

gebiology WILEY

REPORT

Iron-mediated anaerobic ammonium oxidation recorded in the early Archean ferruginous ocean

Alice Pellerin[1] | Christophe Thomazo[1,2] | Magali Ader[3] | Johanna Marin-Carbonne[4] | Julien Alleon[4,5] | Emmanuelle Vennin[1] | Axel Hofmann[6]

[1]Laboratoire Biogéosciences, UMR CNRS 6282, Université de Bourgogne Franche-Comté, Dijon, France

[2]Institut Universitaire de France (IUF), Paris, France

[3]Université Paris Cité, Institut de Physique du Globe de Paris, CNRS, Paris, France

[4]Institut des Sciences de la Terre, University of Lausanne, Lausanne, Switzerland

[5]Université de Lyon, ENS de Lyon, Université Lyon 1, CNRS, LGL-TPE, Lyon, France

[6]Department of Geology, University of Johannesburg, Johannesburg, South Africa

Correspondence
Alice Pellerin, Laboratoire Biogéosciences, UMR CNRS 6282, Université de Bourgogne Franche-Comté, Dijon, France.
Email: alice.pellerin-lefebvre@u-bourgogne.fr

Abstract

The nitrogen isotopic composition of organic matter is controlled by metabolic activity and redox speciation and has therefore largely been used to uncover the early evolution of life and ocean oxygenation. Specifically, positive $\delta^{15}N$ values found in well-preserved sedimentary rocks are often interpreted as reflecting the stability of a nitrate pool sustained by water column partial oxygenation. This study adds much-needed data to the sparse Paleoarchean record, providing carbon and nitrogen concentrations and isotopic compositions for more than fifty samples from the 3.4 Ga Buck Reef Chert sedimentary deposit (BRC, Barberton Greenstone Belt). In the overall anoxic and ferruginous conditions of the BRC depositional environment, these samples yield positive $\delta^{15}N$ values up to +6.1‰. We argue that without a stable pool of nitrates, these values are best explained by non-quantitative oxidation of ammonium via the Feammox pathway, a metabolic co-cycling between iron and nitrogen through the oxidation of ammonium in the presence of iron oxides. Our data contribute to the understanding of how the nitrogen cycle operated under reducing, anoxic, and ferruginous conditions, which are relevant to most of the Archean. Most importantly, they invite to carefully consider the meaning of positive $\delta^{15}N$ signatures in Archean sediments.

KEYWORDS
ammonium oxidation, biogeochemistry, Buck Reef Chert, Feammox, ferruginous ocean, nitrogen isotopes, Paleoarchean

1 | INTRODUCTION

Nitrogen is an essential nutrient for all living organisms, and its availability strongly influences biological productivity. As water column redox speciation controls active metabolic pathways of the biogeochemical nitrogen cycle, the nitrogen isotopic composition of sedimentary rocks can record oceanic redox changes in the early oceans.

On the modern Earth, the atmosphere is the main surface nitrogen reservoir, where N is present mostly as gaseous dinitrogen N_2 (Ward, 2012, $\delta^{15}N = 0‰$). However, nitrogen in its N_2 form can only be assimilated by diazotrophs, prokaryotic organisms who possess the nitrogenase enzyme and are thus capable of biological N_2 fixation (Raymond et al., 2004). Bioavailable "fixed" forms of nitrogen are therefore almost exclusively provided to the biosphere by N_2-fixating

diazotrophs and their mineralization in the water column or in the sediment, referred to as ammonification (Sigman et al., 2009). Fractionations imparted by biological N_2 fixation with classical Mo-based nitrogenase range from −2‰ to +2‰, whereas alternative nitrogenases using Fe or V as cofactors can impart negative fractionations as large as −8‰ (Zhang et al., 2014). In the modern ocean, transfers between the different oceanic nitrogen reservoirs (N_2, NH_4^+, NO_3^- and dissolved and particulate organic nitrogen DON and PON) are mainly controlled by biological processes involving redox reactions. The isotopic composition of these nitrogen sources determines the isotopic composition of primary producers and therefore the sedimentary $\delta^{15}N$. Ammonium release during organic matter remineralization (ammonification) does not impart significant isotope fractionation (Möbius, 2013), and ammonium is rapidly assimilated into the biomass, as it is the preferred inorganic nitrogen source for many organisms. Consequently, even if ammonium assimilation preferentially incorporates ^{14}N, its fractionation is almost never expressed. In oxic conditions prevailing during the Phanerozoic, ammonium can also be successively nitrified to nitrites NO_2^- and nitrates NO_3^-, which are either assimilated by photosynthetic organisms or biologically reduced through denitrification or anaerobic ammonium oxidation (anammox) in dysoxic and anoxic conditions (Dalsgaard & Thamdrup, 2002; Sigman et al., 2009). Denitrification and anammox release N_2O or N_2, which are subsequently lost to the atmosphere, making them the major oceanic sinks of fixed nitrogen. As denitrification imparts a large nitrogen isotope fractionation of ≈30‰ (Sigman et al., 2009), modern and by extension Phanerozoic sedimentary $\delta^{15}N$ values around +5‰ result from the balance between N_2 fixation inputs and denitrification/anammox outputs.

The Archean biogeochemical nitrogen cycle is thought to have been very different from the Phanerozoic, as the redox states of the ocean and the atmosphere have evolved together with rising oxygen levels, impacting environmental conditions and biological evolution. The analysis of 3.5 Ga fluid inclusions containing N_2 (Nishizawa et al., 2007) points toward a stable isotopic composition of atmospheric nitrogen ($\delta^{15}N_{N2}$ = 0‰) at least since the Paleoarchean. Without oxygen levels significant enough to allow nitrification, nitrites and nitrates were likely scarce or absent. Therefore, ammonium is often assumed to have been the dominant form of fixed N prior to the rise of oxygen levels (Beaumont & Robert, 1999; Canfield et al., 2010). Potential abiotic sources of ammonium, including hydrothermal reduction, lightning, and volcanic eruptions, have been reviewed in Stüeken et al. (2016) and their magnitude was deemed too small to have sustained the Archean biosphere. The range of Paleoarchean sedimentary $\delta^{15}N$ values (reviewed in Ader et al., 2016) centers around 0‰, which is compatible with a primitive nitrogen cycle dominated by biological N_2 fixation, ammonification, and ammonium assimilation. The rise of oceanic oxidants preceding the Great Oxidation Event (GOE) might have initiated nitrification/denitrification during the Neoarchean, when positive $\delta^{15}N$ values have been observed (Garvin et al., 2009; Godfrey & Falkowski, 2009; Stüeken et al., 2015; Thomazo et al., 2011), paving the way towards an aerobic nitrogen cycle similar to modern environments.

The first nitrogen isotope Precambrian time series was published by Beaumont and Robert (1999). Since then a lot of data have been acquired but only a few for the Paleoarchean (reviewed in Ader et al., 2016; Mettam & Zerkle, 2021; Stüeken et al., 2016). This is due to the scarcity of well-preserved Paleoarchean geological formations and the difficulty of analyzing nitrogen-poor samples. Therefore, the exceptionally well-preserved and continuous sedimentary record provided by the 900 m BARB3 drill core through the 3.4 Ga Buck Reef Chert offers a unique opportunity to gain some insight into Paleoarchean environments in which an early biosphere could have developed. Moreover, it opens a deep-time window to explore early nitrogen cycle mechanisms such as the onset of N_2 fixation and redox reactions.

2 | GEOLOGICAL CONTEXT

The 3416 ± 5 Ma (Krüner et al., 1991) Buck Reef Chert (BRC) is the largest chert deposit of the Kromberg Formation in the Onverwacht Group, located in the Barberton Greenstone Belt, Kaapvaal craton, South Africa (Lowe & Worrell, 1999). The ICDP-sponsored BARB3 drill core (Hofmann et al., 2013) through the BRC sedimentary deposit records a transition between two sedimentary units: a basal chert-dominated unit from 900 to 600 m depth and a BIF-dominated unit from 600 to 400 m depth. Microscopic observations on the studied BARB3 samples matches detailed facies studies performed on outcrop samples by Tice and Lowe (2006a), except for the evaporitic facies that has not been intersected by the drill core.

The chert-dominated unit consists of a succession of black and white banded cherts with sand-sized carbonaceous grains and laminae, granular cherts, chert breccia and ferruginous cherts with intercalated siderite layers (Figure 1; Figure S1).

The BIF-dominated unit is mainly composed of thick layers of iron-rich carbonates alternating with a smaller proportion of chert beds. Siderite occurs as densely packed rhombic and spherulitic crystals, typical of early diagenetic siderite.

A distinctive feature of the BIF-dominated unit is the occurrence of thin layers ≈1 cm thick of microcrystalline quartz and carbonate characterized by subspherical domains (25 μm) containing micron to sub-micron-sized inclusions of red iron oxides. Single quartz crystals 50 μm in diameter enclose the spheres. These jasper layers are located in the depth intervals of 580–560, 545–500, and 480–400 m (Figure 1, Figure S1). Euhedral iron-rich carbonate crystals in jasper occur in varying amounts (ca. 5%–10%) and are either disseminated or in lenticular clusters, suggesting their early diagenetic nature. The jasper layers are unrelated to any zones where oxic groundwaters could have circulated at depth, which suggests they are primary.

The transition between the chert- and BIF-dominated units is thought to record a temporal and environmental change from a wave-dominated shallow platform to a deeper low-energy basinal depositional environment (Tice & Lowe, 2004) and could also reflect chemical variability linked to an increased supply of dissolved iron through hydrothermal pulses. The origin of the BRC silicified

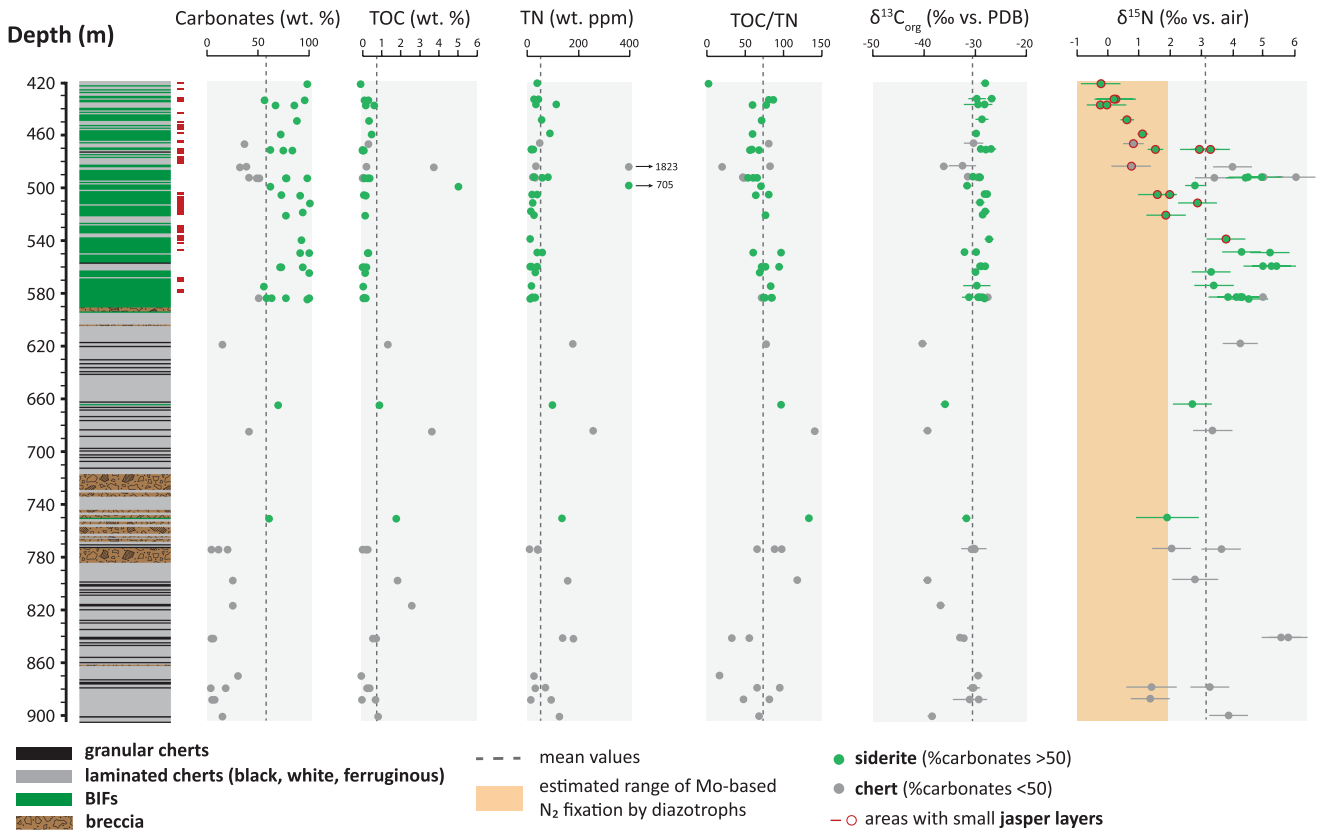

FIGURE 1 Stratigraphic evolution of carbonate content (wt. %), TOC (wt. %), TN (ppm), TOC/TN, $\delta^{13}C_{org}$ (‰ vs. PDB), and $\delta^{15}N$ (‰ vs. air) along the BARB3 drill core.

laminations is variously interpreted in the literature, and four main hypotheses stand out: (i) water column chemical precipitation (Ledevin et al., 2019), (ii) secondary and late silicification of a laminated sedimentary or volcano-sedimentary precursor (de Vries et al., 2006), (iii) segregation from an initial homogenous mix of silica and other components during early diagenesis (Tice & Lowe, 2006a), (iv) pulses of hydrothermal silicification (Geilert et al., 2014). The origin of siderite in the BIF-dominated unit is also debated, as iron-rich carbonates can either precipitate directly in a stratified water column rich in dissolved iron (Klein & Beukes, 1989) or form in the sediment close to the sediment–water interface during diagenesis (Heimann et al., 2010). A hydrothermal origin for siderite has also been suggested for some Archean BIFs (Bolhar et al., 2005).

Regional metamorphism does not exceed the greenschist facies (Tice et al., 2004), with peak temperatures of 310 ± 50°C, according to Raman geothermometry of carbonaceous matter (Alleon et al., 2021).

3 | METHODS

3.1 | Sampling

Fifty-one samples were chosen along the drill core according to their organic matter content (TOC > 0.1% in the digestion residue) that mostly reflects their potential in containing enough nitrogen to analyze. Those samples are composed of various proportions of bands of chert and siderite. Only samples CT6, CT7, and CT18 contain jasper layers. Accordingly, the amount of carbonates in the samples has been used to define two lithological endmembers: "chert" (when carbonates range from 0 to 50 wt. %) and "siderite" (when carbonates range from 50 to 100 wt. %).

3.2 | Mineralogy

Mineralogy was investigated before and after chemical treatment using X-Ray Diffraction (XRD) at the Biogéosciences Laboratory (Université de Bourgogne Franche-Comté, France). Diffractograms were obtained with a Bruker D8 Endeavor diffractometer with CuKα radiation, LynxEye XE-T detector and Ni filter, under 40 kV voltage and 25 mA intensity. The goniometer scanned from 2° to 65° 2θ for each run. Identification of crystalline phases was based on the position and area of their respective mean basal reflections.

3.3 | Chemical treatment

Samples were first crushed into powder using a ring and puck mill at the Biogéosciences Laboratory (Université de Bourgogne Franche-Comté) in order to obtain sample powder smaller than 60 µm. Carbonate-free residues were obtained by mixing sample powders

with 6 N HCl for 24 h, followed by a second step of digestion at 80°C for 4 h. The powder was then rinsed with deionized distilled water to a neutral pH and oven-dried at 40°C for 48 h. Carbonate content, expressed in weight percent (wt. %), was evaluated through gravimetric mass balance after HCl digestion. Some kerogen extracts were commercially produced by Global Geolab Ltd, Alberta, Canada. Powders were digested using HCl and HF, and kerogens were separated out by heavy liquid separation with zinc bromide.

3.4 | C isotopic analyses

The decarbonated residues were poured into tin capsules (20 to 80 mg of powder) and weighted using a Sartorius M2P ultra-balance before TOC and $\delta^{13}C_{org}$ measurements were performed using a Thermo Fisher Scientific Flash Smart elemental analyzer, coupled to a Thermo Fisher Scientific Delta V isotope ratio mass spectrometer (EA-IRMS) via a Conflo IV interface at the Biogéosciences laboratory. Certified USGS40 ($\delta^{13}C_{org} = -26.2‰$, TOC = 40.82 wt. %) and caffeine IAEA-600 ($\delta^{13}C_{org} = -27.77‰$) reference materials were used for the calibration. Total organic carbon (TOC) contents are expressed in dry weight percentage (wt. %) of the non-decarbonated bulk powder and isotope results are reported in delta-notation relative to V-PDB. Each measurement session included three to four standard measurements at the beginning and at the end, as well as one standard measurement every 10 samples. The mean $\delta^{13}C_{org}$ precision for standards is 0.8‰ and the mean accuracy 0.5‰. The number of replicates for each sample is shown in Table 1. The mean external reproducibility (2σ), based on sample replicate analyses and including powder resampling and reprocessing via chemical treatment, is ±0.06 wt. % for the TOC content and ±0.86‰ for the $\delta^{13}C_{org}$. The $\delta^{13}C_{org}$ of 10 kerogen extracts (Table 1) has also been measured following the same procedure mentioned above: their average deviation from corresponding bulk $\delta^{13}C_{org}$ measurements is on average 0.63 ± 0.68‰.

3.5 | N isotopic analyses

As most samples contain less than 200 ppm N (Table 1) and the proportion of silicate-bound nitrogen is unknown, the above-described EA-IRMS method is not sensitive enough for reliable bulk nitrogen isotopic analyses (Ader et al., 2016; Boocock et al., 2020). Samples were therefore analyzed using the "classical method" developed at IPGP described in Ader et al. (2014, 2016), in which N_2 is produced offline through sealed-tube Dumas combustion and cryogenically purified in a vacuum line. Up to 200 mg of decarbonated residual powder was put into a quartz tube with CuO and Cu wires, purified beforehand at 900°C for 2 h in a muffle furnace to prevent contamination. Samples were degassed for 12 h at 150°C under vacuum to remove adsorbed atmospheric N_2 and organics. Quartz tubes were then sealed directly under vacuum and combusted in a muffle furnace at 950°C for 6 h under oxidizing conditions by oxygen liberated from the CuO wires, then cooled at 600°C for 2 h, allowing residual oxygen to combine with cupric oxide and nitrous oxide to be reduced by copper, and finally cooled to ambient temperature (Beaumont & Robert, 1999; Kendall and Grim, 1990). This allows the chemical separation of gaseous products. Busigny et al. (2005) have shown that the extraction yield for this protocol is 100% for both organic and mineral nitrogen, including ammonium in minerals such as phyllosilicates. The content of each quartz tube is liberated in the vacuum line with a tube cracker, where CO_2 and H_2O are trapped cryogenically to avoid any isobaric interferences. The purified incondensable N_2 gas is concentrated into a calibrated volume for quantification using a Toepler pump (Hg manometer). Standard analytical procedures for nitrogen usually include CaO in the reagents to trap gaseous CO_2 and H_2O liberated from samples (Kendall and Grim, 1990), but given that Busigny et al. (2005) have shown that it significantly contributes to analytical blanks, we performed a few tests on samples from the BRC which show that the addition of CaO does not yield significant $\delta^{15}N$ differences. Most samples were consequently analyzed without the addition of CaO, except for the two kerogen extracts. Analytical blanks for the entire procedure are <0.05 micromoles N, which represents less than 10% of the gas for smaller samples and less than 1% for more concentrated samples. Purified N_2 is analyzed by dual-inlet mass spectrometry using a ThermoFinnigan DeltaPlus XP IRMS. Possible air contamination and isobaric interferences due to CO are monitored by scanning of m/z 12 (C from CO_2, CO, CH_4, or organic compounds), 18 (H_2O), 30 ($C^{18}O$), 32 (O_2), 40 (atmospheric Ar), and 44 (CO_2). External $\delta^{15}N$ reproducibility falls between 0.10 and 1.02‰ with a mean of 0.44 ± 0.29‰ ($n = 14$). Samples that were replicated are reported in Table 1. Samples with no external reproducibility are reported with an error of ±0.63‰, which is the external reproducibility of sample 75A replicated 10 times at different concentrations (Table S1). Kerogen extracts of two samples (CT16 and CT18U) yield TN contents and $\delta^{15}N$ values identical within external reproducibility to those measured on their decarbonated counterparts (Table S2).

4 | RESULTS

Iron-rich carbonate throughout the BRC is identified mostly as siderite, with a few samples containing ankerite, based on XRD analyses (Figures S2 and S3 ; Table S3), which is consistent with previous investigations (Tice et al., 2004; Tice & Lowe, 2006a; Tice & Lowe, 2006b). Carbonate content obtained through HCl digestion is highly variable (2% to 99%) depending on the relative proportions of bands of chert versus siderite. Total organic carbon (TOC) contents vary between 0.01% and 5.01% with a mean value of 0.66 ± 1.01% ($n = 52$). Total nitrogen (TN) content ranges from 11 to 259 ppm with a mean of 55 ± 53 ppm ($n = 55$), excluding two N-rich outliers (samples 75A and 73A showing TN contents of 1823 and 705 ppm, respectively). TOC/TN ratios are below 150, which is relatively low for Archean sedimentary rocks (Yamaguchi, 2002); it ranges from 3 to 141 with a mean TOC/TN of 72 ± 24 ($n = 51$).

TABLE 1 Summary data table featuring the depth (m), carbonate content (wt. %), TOC (wt. %) with its standard deviation (SD) and number of replicates, TN (wt. ppm) with its standard deviation (SD) and number of replicates, TOC/TN, $\delta^{13}C_{org}$ (‰ vs. PDB) with its standard deviation (SD) and number of replicates, $\delta^{13}C_{ker}$ (‰ vs. PDB), and $\delta^{15}N$ (‰ vs. air) with its standard deviation (SD) and number of replicates, for each sample analyzed along the BARB3 drill core.

Sample	Depth (m)	Carbonate content (wt. %)	TOC (wt. %)	SD	Nb repl.	TN (wt. ppm)	SD	Nb repl.	TOC/TN	$\delta^{13}C_{org}$ (‰ vs. PDB)	SD	Nb repl.	$\delta^{15}N$ (‰ vs. air)	SD	Nb repl.
27A[a]	421.37	96	0.01		1	41		1	3	−27.96	0.84	1	−0.3	0.63	1
CT19U[a]	433.18	93	0.40	0.14	2	45		1	87	−26.68	0.84	1	0.2	0.63	1
CT19L[a]	433.24	54	0.21	0.02	3	26		1	81	−29.58	1.73	3	0.2	0.63	1
CT18U[a]	437.27	83	0.69	0.21	2	114	3	2	60	−28.13	0.35	2	−0.3	0.10	2
CT18L[a]	437.36	65	0.28	0.02	3	35		1	78	−29.37	2.77	3	−0.1	0.63	1
CT17[a]	448.64	86	0.42	0.07	3	58	3	3	73	−28.59	1.23	2	0.6	0.22	3
CT16[a]	459.03	70	0.55	0.15	2	90	5	3	61	−29.78	0.39	2	1.1	0.18	3
CT15[a]	466.33	35	0.41	0.01	3	50		1	81	−30.23	1.93	3	0.8	0.34	2
CT14U[a]	470.82	60	0.11	0.02	3	18		1	60	−28.81	0.39	2	3.3	0.63	1
CT14M[a]	470.94	81	0.10	0.01	3	18	1	2	57	−26.82	1.11	3	1.5	0.25	2
CT14L[a]	471.05	73	0.17	0.02	3	24		1	69	−27.84	0.40	3	2.9	0.63	1
CT13[a]	483.39	36	0.30	0.15	3	36	3	2	83	−32.45	2.69	3	0.7	0.64	2
75A	483.81	30	3.77		1	1823	96	10	21	−36.11	0.84	1	4.0	0.63	10
CT5U_U	491.66	39	0.14	0.04	3	29		1	48	−31.42	0.29	3	6.1	0.63	1
CT5U_M	491.74	75	0.45	0.09	3	82		1	55	−30.43	0.83	3	4.5	0.63	1
CT5U_L	491.82	47	0.11	0.01	3	22		1	49	−29.17	0.21	3	5.0	0.63	1
CT5L_U	491.9	76	0.18	0.02	3	28		1	66	−29.14	0.17	3	4.9	0.63	1
CT5L_M	491.98	49	0.16	0.03	3	32		1	49	−29.54	0.22	3	3.4	0.63	1
CT5L_L	492.04	96	0.37	0.25	2	61		1	61	−28.93	0.71	2	4.4	0.63	1
73A	498.09	60	5.01		1	705	34	3	71	−31.53	0.84	1	2.8	0.31	3
CT6U[a]	504.68	71	0.16	0.01	3	20		1	82	−27.51	0.36	3	1.6	0.63	1
CT6L[a]	504.8	89	0.26	0.08	3	40	2	2	65	−28.13	0.36	3	2.0	0.19	2
72B[a]	511.05	99				23		1		−28.97	0.84	1	2.9	0.63	1
21A	517.53	92				16		1		−27.91	0.84	1			
CT7[a]	520.05	75	0.22	0.01	3	28		1	77	−28.44	0.61	3	1.9	0.63	1
20A[a]	538.26	90				13		1		−27.17	0.84	1	3.8	0.63	1
CT12U	548.08	98	0.37	0.28	2	60		1	61	−29.80	0.84	1	4.3	0.63	1
CT12L	548.15	89	0.38	0.03	3	40		1	97	−32.08	0.19	3	5.2	0.63	1
CT11U	558.62	70	0.16	0.01	3	17		1	95	−27.93	0.50	3	5.3	0.63	1

(Continues)

TABLE 1 (Continued)

Sample	Depth (m)	Carbonate content (wt. %)	TOC (wt. %)	SD	Nb repl.	TN (wt. ppm)	SD	Nb repl.	TOC/TN	$\delta^{13}C_{org}$ (‰ vs. PDB)	SD	Nb repl.	$\delta^{15}N$ (‰ vs. air)	SD	Nb repl.
CT11M	558.68	92	0.31	0.04	3	40		1	77	−29.01	0.25	3	5.0	0.63	1
CT11L	558.75	71	0.09	0.02	3	13		1	73	−28.68	0.15	3	5.4	0.63	1
CT10	562.96	98	0.23	0.08	3	32		1	70	−29.82	0.01	2	3.3	0.63	1
CT9	573.11	54	0.14	0.00	3	17		1	84	−29.62	2.69	3	3.4	0.63	1
CT8U_U	581.76	61	0.17	0.05	3	23	4	2	76	−31.16	1.42	3	4.1	0.63	1
CT8U_L	581.88	49	0.14	0.01	3	20	2	3	72	−27.48	0.20	3	5.0	0.12	2
CT8L_U	581.93	98	0.27	0.05	3	32		1	85	−28.43	0.84	1	4.3	0.63	1
CT8L_M	581.96	75	0.18	0.01	3	21		1	85	−28.92	0.28	3	4.3	0.63	1
CT8L_L	582	56	0.23	0.02	3	30		1	75	−29.31	0.14	3	3.9	0.63	1
18A	583.03	96				12		1		−28.10	0.84	1	4.5	0.63	1
17A	616.77	13	1.41		1	180	7	3	78	−40.35	0.84	1	4.3	0.57	3
16A	662.32	68	0.96		1	99		1	98	−35.91	0.84	1	2.7	0.63	1
61A	682	39	3.65		1	259		1	141	−39.40	0.84	1	3.4	0.63	1
58A	747.59	59	1.83		1	137		2	134	−31.72	0.84	1	1.9	1.02	2
CT4U	770.65	19	0.11	0.04	2	11		1	99	−30.18	2.47	2			
CT4L_U	770.8	9	0.37	0.05	2	41		1	89	−30.01	0.33	2	2.0	0.63	1
CT4L_L	770.95	2	0.28	0.00	3	42		1	66	−30.68	0.03	2	3.6	0.63	1
9A	794.12	23	1.89		1	159	2	2	118	−39.39	0.84	1	2.8	0.75	2
52A	813.05	23	2.61		1					−36.77	0.84	1			
CT3U	837.32	4	0.78	0.03	2	140		1	56	−33.01	0.32	2	5.8	0.63	1
CT3L	837.51	3	0.62	0.06	2	181		1	34	−32.15	0.45	2	5.6	0.63	1
49A	865.76	29	0.05		1	27	18	2	17	−29.37	0.84	1			
CT2U	874.65	2	0.47	0.06	2	71		1	66	−30.52	0.99	2	3.3	0.63	1
CT2L	874.87	16	0.32	0.01	2	33	4	3	96	−30.24	1.28	2	1.4	0.82	2
CT1U	883.47	6	0.78	0.05	2	94		1	83	−30.99	3.43	2	1.3	0.63	1
CT1L	883.65	3	0.08	0.01	2	16		1	49	−29.25	0.04	2			
1A	896	13	0.88		1	128		1	69	−38.49	0.84	1	3.9	0.63	1

[a]Samples containing jasper layers.

Note: Green shade indicates Cherts (carbonates <50 wt. %); Grey shade indicates Siderites (carbonates >50 wt. %).

Along the drill core, $\delta^{15}N$ values ($n = 51$) range between −0.3‰ and + 6.1‰ with a mean $\delta^{15}N$ of 3.1 ± 1.8‰. $\delta^{15}N$ variations are not correlated with either organic carbon ($R^2 = .0308$) or nitrogen concentrations ($R^2 = .0043$) (Figure 3). The average $\delta^{15}N$ value in the chert-dominated unit does not significantly differ from the average $\delta^{15}N$ value in the BIF-dominated unit, nor do $\delta^{15}N$ values in chert samples significantly differ from $\delta^{15}N$ values in siderite samples (Figure 2, $p > .05$). However, $\delta^{15}N$ values ($n = 17$) from the BIF-dominated unit with jasper layers are significantly different (Figure 2, $p < .05$) from $\delta^{15}N$ values ($n = 34$) in core intervals lacking jasper, with a mean $\delta^{15}N$ of 1.3‰ and 4.0‰ respectively. $\delta^{15}N$ values display stratigraphic variations along the BARB3 drill core, with markedly positive values in most of the core, and values decreasing toward 0‰ in the upper part, between depths of 400 and 500 m.

$\delta^{13}C_{org}$ in the BIF-dominated unit and in the chert-dominated unit show close mean values of −29.3 ± 1.8‰ ($n = 39$) and −33.4 ± 4.0‰ ($n = 17$) respectively, but the latter displays a much larger range of variations (from −40.4‰ to −29.3‰), whereas values in the BIF-dominated unit are much more homogenous (from −32.5‰ to −26.7‰ leaving out one outlier). The same $\delta^{13}C_{org}$ variations hold true for chert and siderite samples (Figure 2).

5 | DISCUSSION

The potential impact of post-depositional processes on the $\delta^{15}N$ is discussed in Supplementary Information. All indicators point to a good preservation of the BRC samples primary nitrogen isotopic signature. Besides, even if metamorphic processes in the greenschist facies may have slightly shifted the $\delta^{15}N$ (<2‰), they cannot account for the large range of values observed in the BRC and their rapid stratigraphic variations.

5.1 | A biotic organic source of N

Nitrogen-bearing organic molecules produced in organic hazes such as in Titan's atmosphere (tholins) are mentioned as an abiotic alternative to organic matter production during the Archean (Izon et al., 2015; Trainer et al., 2006). However, organic molecules generated through experimental aerosols production setups in plasma or photochemical flow reactors are depleted in ^{15}N (from 0.8‰ to −25.5‰) compared with the initial N_2 gas from which they precipitated (Kuga et al., 2014; Sebree et al., 2016). If the $\delta^{15}N_{N2}$ value of the Archean atmosphere was similar to that of the present-day atmosphere ($\delta^{15}N_{N2} = 0‰$, Nishizawa et al., 2007), then the range of $\delta^{15}N$ values observed in the BRC is not consistent with a significant contribution of ^{15}N-depleted abiotic organic matter. The relatively stable TN along the drill core would also mean a sustained abiotic production of these organic molecules, which seems unlikely given the suggested rapid oscillations between hazy and haze-free states evidenced for the Neoarchean atmosphere (Izon et al., 2015; Zerkle et al., 2012). Indeed, oscillations that have only been observed over stratigraphic intervals of a few dozens of meters are hard to reconcile with the 350 m-thick BRC, even if the sedimentation rate remains poorly constrained.

While hydrothermal activity may have been widespread on Archean oceans seafloor and fluid circulations have likely

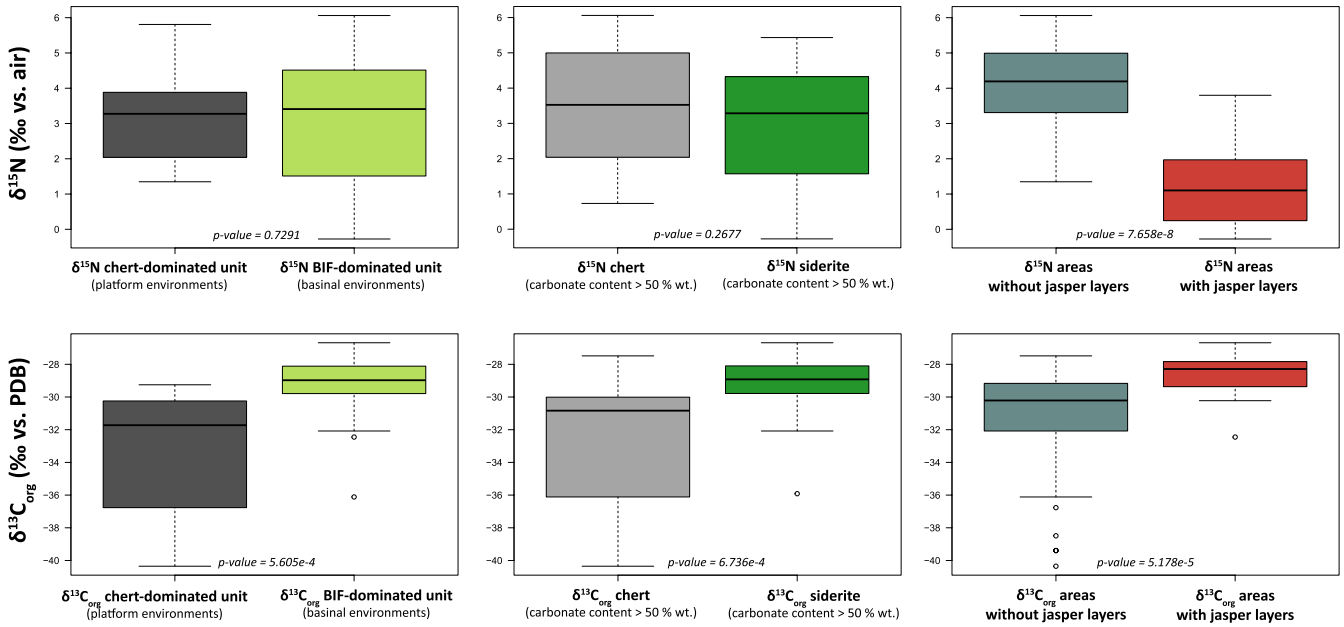

FIGURE 2 Boxplots showing the $\delta^{15}N$ and $\delta^{13}C_{org}$ range of values and means between (1) the chert-dominated unit and the BIF-dominated unit, (2) chert samples and siderite samples and (3) areas of the drill core with or without jasper layers.

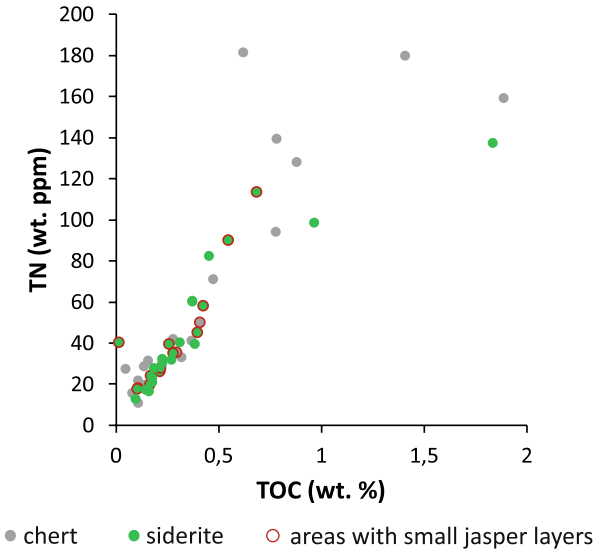

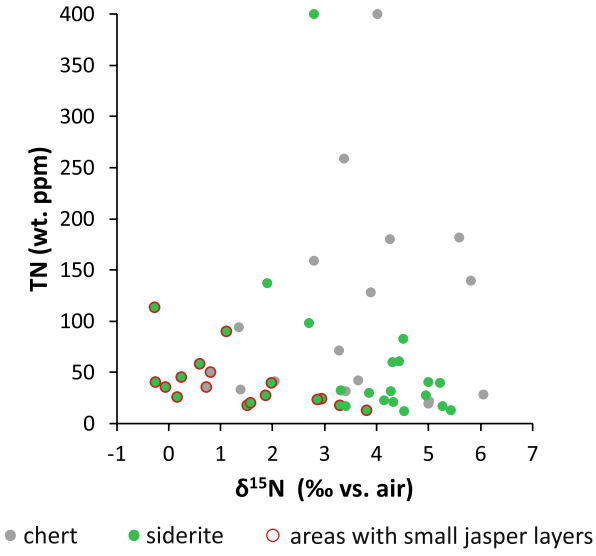

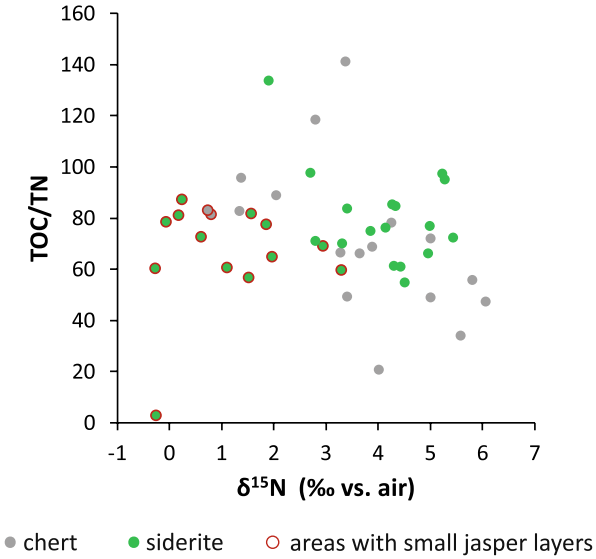

FIGURE 3 Crossplots: TOC (wt. %) vs. TN (wt. ppm); $\delta^{15}N$ (‰ vs. air) vs. TN (wt. ppm); $\delta^{15}N$ (‰ vs. air) vs. TOC/TN.

influenced the availability of nutrients like dissolved iron (Poulton & Canfield, 2011), it seems unlikely that hydrothermal circulations either made a strong contribution of abiotic organic nitrogen to the BRC or that it significantly shifted its bulk $\delta^{15}N$ signal. Indeed, the contribution of mantellic N to hydrothermal systems seems low compared to hydrothermal remobilization of previously sedimented nitrogen (Stüeken et al., 2021). Neither typical mantellic $\delta^{15}N$ values around −5‰ (Cartigny & Marty, 2013) nor $\delta^{15}N$ values measured for altered oceanic crust (ranging from −12‰ to +8‰, Li et al., 2007) have been found in the BRC samples. Instead, the BRC lowest $\delta^{15}N$ values are consistent with the range of fractionation displayed by Mo-based biological fixation of N_2 by diazotrophs (Nishizawa et al., 2014; Sigman et al., 2009; Zhang et al., 2014).

Abiotic graphite formation has been identified in highly metamorphosed, siderite-bearing sedimentary rocks of the Eoarchean Isua Supracrustal Belt (van Zuilen et al., 2003). In the BRC, organic matter is not preferentially associated with siderite layers, which suggests that it was not formed by thermal decomposition of siderite.

Therefore, the most probable hypothesis is that nitrogen found in the BRC samples has a biotic source, namely biological N_2 fixation by diazotrophs in the photic zone, followed by organic matter mineralization in the water column or the sediment.

5.2 | Anoxic and reducing paleoenvironmental conditions

The lithologies of the BRC (mainly chert and siderite), the lack of Ce anomalies (Tice & Lowe, 2006b), and the presence of mass-independent fractionation of sulfur isotopes in sulfides (S-MIF, Galić, 2015) are consistent with overall reducing and anoxic conditions. The thin jasper layers within the BIF-dominated unit indicate that iron oxidation may nonetheless have taken place punctually, possibly due to anoxygenic photosynthesis (Tice & Lowe, 2006b) or UV photolysis (Konhauser et al., 2007).

The Archean ocean was likely saturated in silica, which either could have precipitated in the water column or formed silica gels at the sediment surface (Ledevin et al., 2019). The main iron source in Archean oceans is likely Fe(II) provided by hydrothermalism (Poulton & Canfield, 2011). The siderite enrichment in the BIF-dominated unit could either indicate deepening of the water column such that the depositional setting was overlain by Fe(II)-rich bottom waters in a stratified ocean (Tice & Lowe, 2004), or periods of increased hydrothermal activity releasing large quantities of dissolved Fe, indicating a chemical shift from a silica-rich to a carbonate-rich fluid.

5.3 | Nitrogen cycling in the Paleoarchean BRC

In the anoxic and ferruginous environmental context of the BRC, nitrites and nitrates would not have been thermodynamically stable. Therefore, the water column nitrogen pool was most probably fixed ammonium (Beaumont & Robert, 1999; Canfield et al., 2010), either released during the degradation of organic matter or released from lithified sediments through fluid circulations (Stüeken et al., 2021).

Nevertheless, nitrification in a stratified ocean with an oxic surface layer has been proposed for some Neoarchean and Paleoproterozoic settings (Garvin et al., 2009; Godfrey & Falkowski, 2009; Kipp et al., 2018; Koehler et al., 2018). While the production of small amounts of nitrates cannot be fully ruled out, it is unlikely that nitrification could have been sustained in the reducing and anoxic conditions of the depositional environment of the Paleoarchean BRC. Indeed, an anoxic atmosphere evidenced by the S-MIF data (Galić, 2015) seems incompatible with an oceanic surface layer hosting a stable nitrate reservoir. In addition, the small range of pyrites $\delta^{34}S$ values (Galić, 2015) indicate that sulfates were scarce, further supporting the absence of significant concentrations of oxidized anions in the BRC water column. Therefore, without a stable pool of nitrates that could explain the enrichment in ^{15}N of a residual nitrate pool through denitrification and its subsequent assimilation by primary producers, a mechanism that can fractionate NH_4^+ before its assimilation is required to explain the observed positive nitrogen isotopic signatures.

Partial biological assimilation of NH_4^+ can enrich residual organic matter in ^{14}N ($\varepsilon \approx -4‰$ to $-27‰$, Hoch et al., 1992), if the pool of ammonium is not quantitatively consumed, which might be possible in upwelling regions. However, the expected distribution of $\delta^{15}N$ values should be centered around 0‰, displaying both the upwelled ^{15}N-depleted and the sinking ^{15}N-enriched pools of ammonium. While this mechanism has been proposed to explain the negative and near zero $\delta^{15}N$ values found in the Paleoarchean (Ader et al., 2016; Beaumont & Robert, 1999), $\delta^{15}N$ values in the BRC are centered around 3.3‰ with no negative values. This means that in the BRC depositional environment, an additional mechanism enriching residual ammonium in ^{15}N was operating at a regional scale.

The hypothesis of positive ammonium $\delta^{15}N$ values resulting from NH_3 degassing at high pH (Stüeken et al., 2015) (pH>9.2) is compatible with the precipitation of iron-rich carbonates but seems unlikely in the context of the BRC given that positive $\delta^{15}N$ values are also found in chert layers (Figure 1), which require decreasing pH values (Wright, 2022).

The oxidation of ammonium is therefore the only remaining mechanism capable of producing a $^{15}NH_4^+$-enriched pool that could have been recorded in the BRC organic N after assimilation.

Most metabolic pathways oxidizing NH_4^+ need free O_2, and even classic anaerobic ammonium oxidation (anammox) requires the presence of nitrites, which cannot be produced without O_2 (Grotzinger & Kasting, 1993). However, in anoxic and ferruginous conditions, NH_4^+ can be oxidized to N_2 in the presence of iron oxides through the Feammox reaction (Stüeken et al., 2016):

$$6\,Fe(OH)_3 + 2\,NH_4^+ + 10\,H^+ \rightarrow 6\,Fe^{2+} + N_2 + 18\,H_2O$$

This reaction has only recently been described in modern environments, namely in iron-rich conditions in wetland soils and marine sediments (Rios-Del Toro et al., 2018; Yang et al., 2012). Such a metabolism is compatible with Eh-pH conditions and iron speciation during the Archean period, as it is thermodynamically favored when Fe^{2+} concentrations are below 100 μM and NH_4^+ concentrations are above 1 μM, for pH between 6 and 8 (Stüeken et al., 2016). These conditions were probably achieved in the Paleoarchean seafloor, given the available constraints on its pH values around 6.5 to 7 (Halevy & Bachan, 2017). Ammonium and iron concentrations measured in modern anoxic and ferruginous environments (Petrash et al., 2022) and estimated for ancient environments (Canfield, 2005; Tosca et al., 2019) are also in accordance with this hypothesis.

Jasper layers observed in the BRC suggest that iron redox cycling (from anoxygenic photosynthesis or UV photolysis) was occurring and could have provided iron oxides to the Feammox reaction. Ammonium released from biomass degradation during diagenesis could have been in direct contact with iron oxides in the sediment, allowing Feammox to operate while residual ^{15}N-enriched ammonium could have exchanged isotopically with organic matter or been assimilated by benthic organisms. Feammox is also capable of producing N_2 at rates that can outcompete denitrification in iron-rich tropical soils (Yang et al., 2012). It therefore provides a return nitrogen flux to the atmosphere before the spread of denitrification, which is consistent with a stable atmospheric N_2 reservoir from 3.5 Ga (Nishizawa et al., 2007).

While the fractionation factor for Feammox remains to be determined, all known ammonium oxidation pathways enrich residual NH_4^+ in ^{15}N. In particular, anammox fractionation can equal that of denitrification (Brunner et al., 2013). The assimilation of the residual ^{15}N-enriched ammonium into the biomass will then lead to positive sedimentary $\delta^{15}N$ values (Figure 4).

Such positive values in the BRC are observed where jasper layers are absent, indicating limited iron oxide availability and/or reduction in those iron oxides by reactions with organic matter or sulfide during diagenesis. By contrast, the lowest $\delta^{15}N$ values are observed in the intervals of the BIF-dominated unit that contain jasper layers, that is, in environments where iron oxides were either abundant or well preserved. The return to a diazotrophic environment could either mean that the Feammox reaction did not take place in settings where waters were saturated in Fe^{2+} to concentrations capable of inhibiting this metabolic pathway or that iron oxides were not scavenged by sulfides and abundant enough to allow NH_4^+ to be entirely consumed by the Feammox reaction, leaving no detectable fractionation (Figure 4).

As to organic carbon isotopic signatures, $\delta^{13}C_{org}$ values in the BIF-dominated unit are centered around −30‰, which is consistent with carbon fixation through the Calvin cycle, a pathway that exists in both chemoautotrophs and photosynthesizers, either anoxygenic or oxygenic. Such values fall in the typical range for photosynthesis,

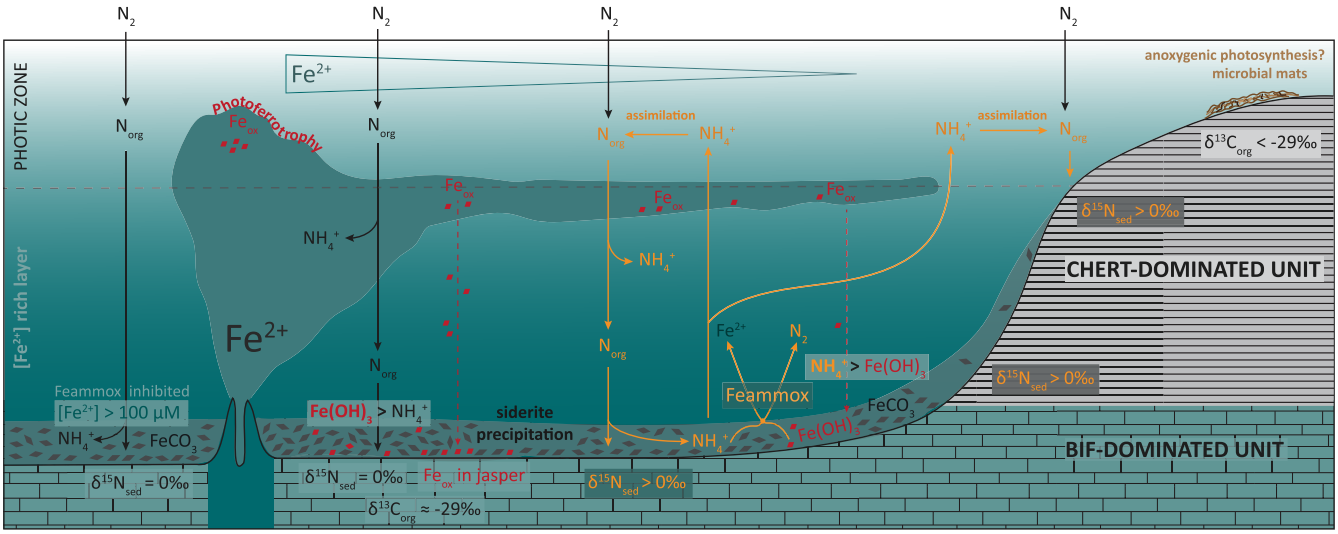

FIGURE 4 Schematic model illustrating how the iron and nitrogen cycles could have interacted in an anoxic and ferruginous Archean ocean, as recorded in the BRC formation. Following the sedimentary model described by Tice and Lowe (2004), the chert-dominated unit is related to platform settings and gives way to the BIF-dominated unit as depth increases toward basin settings. The water column is chemostratified, with a lower Fe^{2+}-rich layer supplied by hydrothermal iron fluxes. Siderite precipitates either at the chemocline or in the sediment and accumulates on the seafloor, forming the BIF-dominated unit. The abundance of siderite follows a gradient away from the hydrothermal discharge zones. In the absence of free O_2 in the water column, iron oxides observed in the BRC jasper layers can be produced through photoferrotrophy when dissolved Fe^{2+} reaches the photic zone. Organic nitrogen is sourced to the water column by diazotrophic N_2 fixation and is either consumed by organisms or ammonified as NH_4^+. In the chert-dominated unit, iron oxides are scarce and therefore quantitatively consumed by Feammox. The residual ammonium becomes enriched in ^{15}N and can carry this enrichment to organic matter when reassimilated, which would produce positive sedimentary $\delta^{15}N$ values. In the iron-rich settings of the BIF-dominated unit, $\delta^{15}N$ values are close to 0‰, recording only biological N_2 fixation by diazotrophs. This could either result from quantitative consumption of NH_4^+ by Feammox due to an excess of iron oxides or to an inhibition of Feammox by dissolved Fe^{2+} concentrations exceeding 100 µM.

likely anoxygenic given other oxidation indicators. The chert-dominated unit displays more variable $\delta^{13}C_{org}$ values, which points toward a larger diversity of metabolisms in shallow depositional environments, possibly within benthic communities of biomats (Tice & Lowe, 2004). Some of the strongly negative values, down to −40‰, are consistent with methanotrophy/methanogenesis, which is all the more interesting because iron oxides can also be used to oxidize methane (Lepot, 2020). These strongly negative $\delta^{13}C_{org}$ values are thus consistent with Fe(III)-driven oxidation of organic products, including methane and ammonium.

6 | CONCLUSION

Carbon and nitrogen isotopic compositions in the 3.4 Ga Buck Reef Chert display a large range of variations. However, while the sedimentary $\delta^{13}C_{org}$ signal seems to change with the depositional environment or chemical conditions, the bulk sedimentary $\delta^{15}N$ signal seems to rather primarily reflect iron oxides availability. $\delta^{15}N$ values are consistently positive and reach up to +6.1‰ in both jasper-free cherts and siderites of the two main sedimentary units, whereas they display a distinctive diazotrophic Mo-based N_2 fixation signature close to 0‰ in the jasper-bearing facies of the upper BIF-dominated unit. Positive $\delta^{15}N$ values observed in sediments that are more scarce in iron could have resulted from the partial oxidation of NH_4^+ to N_2 through the Feammox reaction, whereas sediments deposited in an environment saturated in Fe^{2+} would show no isotopic nitrogen fractionation, either from direct Feammox inhibition or from complete consumption of the ammonium pool. Accordingly, these findings suggest that iron availability could have controlled the nitrogen isotopic signature recorded in sediments through an ammonium oxidative pathway. More importantly, these results call for careful consideration of the meaning of positive $\delta^{15}N$ signatures in Archean ferruginous sediments. Indeed, while ^{15}N-enriched sedimentary organic matter has often been used as a redox indicator of a stable pool of nitrates in "oxygen oases," this study shows that in anoxic settings where Fe(III) minerals are present, the oxidation of ammonium can lead to similar positive $\delta^{15}N$ signatures. As anoxic and ferruginous conditions are thought to have been widespread in the Archean ocean, it might be necessary to carefully consider iron abundance and speciation when interpreting the nitrogen isotopic signatures and to rely on complementary redox indicators.

ACKNOWLEDGMENTS

This work is a contribution to the Institut Universitaire de France project EVOLINES. It was supported by the Observatoire des Sciences de l'Univers Terre Homme Environnement Temps Astronomie of Bourgogne-Franche-Comté (OSU THETA). For technical support, the authors would like to thank Anne-Lise Santoni, Ludovic Bruneau and the GISMO platform (Université de Bourgogne Franche-Comté,

France), and Virginia Rojas (Institut de Physique du Globe de Paris, France). AH acknowledges the DSI-NRF Centre of Excellence in Palaeosciences (Grant 86073). Drilling in the Barberton greenstone belt was supported by the International Continental Scientific Drilling Program (ICDP). JMC acknowledges the innovation program ERC (STROMATA, grant agreement 759289).

DATA AVAILABILITY STATEMENT

The data that supports the findings of this study are available in the supplementary material of this article.

ORCID

Alice Pellerin https://orcid.org/0000-0001-6828-5899
Magali Ader https://orcid.org/0000-0002-9239-1509
Johanna Marin-Carbonne https://orcid.org/0000-0002-4265-1595

REFERENCES

Ader, M., Thomazo, C., Sansjofre, P., Busigny, V., Papineau, D., Laffont, R., Cartigny, P., & Halverson, G. P. (2016). Interpretation of the nitrogen isotopic composition of Precambrian sedimentary rocks: Assumptions and perspectives. *Chemical Geology*, *429*, 93–110. https://doi.org/10.1016/j.chemgeo.2016.02.010

Alleon, J., Bernard, S., Olivier, N., Thomazo, C., & Marin-Carbonne, J. (2021). Inherited geochemical diversity of 3.4 Ga organic films from the Buck Reef Chert. *South Africa. Communications Earth & Environment*, *2*, 1–7. https://doi.org/10.1038/s43247-020-00066-7

Beaumont, V., & Robert, F. (1999). Nitrogen isotope ratios of kerogens in Precambrian cherts: A record of the evolution of atmosphere chemistry? *Precambrian Research*, *96*, 63–82. https://doi.org/10.1016/S0301-9268(99)00005-4

Bolhar, R., Van Kranendonk, M. J., & Kamber, B. S. (2005). A trace element study of siderite–jasper banded iron formation in the 3.45Ga Warrawoona group, Pilbara craton—Formation from hydrothermal fluids and shallow seawater. *Precambrian Research*, *137*, 93–114. https://doi.org/10.1016/j.precamres.2005.02.001

Boocock, T. J., Mikhail, S., Prytulak, J., Di Rocco, T., & Stüeken, E. E. (2020). Nitrogen mass fraction and stable isotope ratios for fourteen geological reference materials: Evaluating the applicability of elemental Analyser versus sealed tube combustion methods. *Geostandards and Geoanalytical Research*, *44*, 537–551 10.1111/ggr.12345

Brunner, B., Contreras, S., Lehmann, M. F., Matantseva, O., Rollog, M., Kalvelage, T., Klockgether, G., Lavik, G., Jetten, M. S. M., Kartal, B., & Kuypers, M. M. M. (2013). Nitrogen isotope effects induced by anammox bacteria. *Proceedings of the National Academy of Sciences of the United States of America*, *110*, 18994–18999. https://doi.org/10.1073/pnas.1310488110

Busigny, V., Ader, M., & Cartigny, P. (2005). Quantification and isotopic analysis of nitrogen in rocks at the ppm level using sealed tube combustion technique: A prelude to the study of altered oceanic crust. *Chemical Geology*, *223*, 249–258 10.1016/j.chemgeo.2005.08.002

Canfield, D. E. (2005). THE EARLY HISTORY OF ATMOSPHERIC OXYGEN: Homage to Robert M. Garrels. *Annual Review of Earth and Planetary Sciences*, *33*, 1–36. https://doi.org/10.1146/annurev.earth.33.092203.122711

Canfield, D. E., Glazer, A. N., & Falkowski, P. G. (2010). The evolution and future of Earth's nitrogen cycle. *Science*, *330*, 192–196. https://doi.org/10.1126/science.1186120

Cartigny, P., & Marty, B. (2013). Nitrogen isotopes and mantle geodynamics: The emergence of life and the atmosphere–crust–mantle connection. *Elements*, *9*, 359–366. https://doi.org/10.2113/gselements.9.5.359

Dalsgaard, T., & Thamdrup, B. (2002). Factors controlling anaerobic ammonium oxidation with nitrite in marine sediments. *Applied and Environmental Microbiology*, *68*, 3802–3808. https://doi.org/10.1128/AEM.68.8.3802-3808.2002

e Vries, S. T., Nijman, W., & Armstrong, R. A. (2006). Growth-fault structure and stratigraphic architecture of the Buck Ridge volcano-sedimentary complex, upper Hooggenoeg formation, Barberton Greenstone Belt, South Africa. *Precambrian Research*, *149*, 77–98. https://doi.org/10.1016/j.precamres.2006.04.005

Galić, A. (2015). *Unravelling atmospheric photolysis and ocean redox chemistry from Paleoarchean pyrite: A multiple sulfur and iron stable isotope study*. PhD thesis. Universiteit Utrecht.

Garvin, J., Buick, R., Anbar, A. D., Arnold, G. L., & Kaufman, A. J. (2009). Isotopic evidence for an aerobic nitrogen cycle in the latest Archean. *Science*, *323*, 1045–1048. https://doi.org/10.1126/science.1165675

Geilert, S., Vroon, P. Z., & van Bergen, M. J. (2014). Silicon isotopes and trace elements in chert record early Archean basin evolution. *Chemical Geology*, *386*, 133–142. https://doi.org/10.1016/j.chemgeo.2014.07.027

Godfrey, L. V., & Falkowski, P. G. (2009). The cycling and redox state of nitrogen in the Archaean ocean. *Nature Geoscience*, *2*, 725–729. https://doi.org/10.1038/ngeo633

Grotzinger, J. P., & Kasting, J. F. (1993). New constraints on Precambrian ocean composition. *The Journal of Geology*, *101*, 235–243. https://doi.org/10.1086/648218

Halevy, I., & Bachan, A. (2017). The geologic history of seawater pH. *Science*, *355*, 1069–1071. https://doi.org/10.1126/science.aal4151

Heimann, A., Johnson, C. M., Beard, B. L., Valley, J. W., Roden, E. E., Spicuzza, M. J., & Beukes, N. J. (2010). Fe, C, and O isotope compositions of banded iron formation carbonates demonstrate a major role for dissimilatory iron reduction in ~2.5Ga marine environments. *Earth and Planetary Science Letters*, *294*, 8–18. https://doi.org/10.1016/j.epsl.2010.02.015

Hoch, M. P., Fogel, M. L., & Kirchman, D. L. (1992). Isotope fractionation associated with ammonium uptake by a marine bacterium. *Limnology and Oceanography*, *37*, 1447–1459. https://doi.org/10.4319/lo.1992.37.7.1447

Hofmann, A., Karykowski, B., Mason, P., Chunnet, G., & Arndt, N. (2013). *Barberton drilling project - Buck Reef Chert core BARB3*. 15, EGU2013-12227.

Izon, G., Zerkle, A. L., Zhelezinskaia, I., Farquhar, J., Newton, R. J., Poulton, S. W., Eigenbrode, J. L., & Claire, M. W. (2015). Multiple oscillations in Neoarchaean atmospheric chemistry. *Earth and Planetary Science Letters*, *431*, 264–273. https://doi.org/10.1016/j.epsl.2015.09.018

Kendall, C., & Grim, E. (1990). Combustion tube method for measurement of nitrogen isotope ratios using calcium oxide for total removal of carbon dioxide and water. *Analytical Chemistry*, *62*, 526–529.

Kipp, M. A., Stüeken, E. E., Yun, M., Bekker, A., & Buick, R. (2018). Pervasive aerobic nitrogen cycling in the surface ocean across the Paleoproterozoic era. *Earth and Planetary Science Letters*, *500*, 117–126. https://doi.org/10.1016/j.epsl.2018.08.007

Klein, C., & Beukes, N. J. (1989). Geochemistry and sedimentology of a facies transition from limestone to iron-formation deposition in the early Proterozoic Transvaal supergroup, South Africa. *Economic Geology*, *84*, 1733–1774. https://doi.org/10.2113/gsecongeo.84.7.1733

Koehler, M. C., Buick, R., Kipp, M. A., Stüeken, E. E., & Zaloumis, J. (2018). Transient surface ocean oxygenation recorded in the ~2.66-Ga Jeerinah formation, Australia. *Proceedings of the National Academy of Sciences*, *115*, 7711–7716. https://doi.org/10.1073/pnas.1720820115

Konhauser, K. O., Amskold, L., Lalonde, S. V., Posth, N. R., Kappler, A., & Anbar, A. (2007). Decoupling photochemical Fe(II) oxidation from

shallow-water BIF deposition. *Earth and Planetary Science Letters*, *258*, 87–100. https://doi.org/10.1016/j.epsl.2007.03.026

Krüner, A., Byerly, G. R., & Lowe, D. R. (1991). Chronology of early Archaean granite-greenstone evolution in the Barberton Mountain land, South Africa, based on precise dating by single zircon evaporation. *Earth and Planetary Science Letters*, *103*, 41–54. https://doi.org/10.1016/0012-821X(91)90148-B

Kuga, M., Carrasco, N., Marty, B., Marrocchi, Y., Bernard, S., Rigaudier, T., Fleury, B., & Tissandier, L. (2014). Nitrogen isotopic fractionation during abiotic synthesis of organic solid particles. *Earth and Planetary Science Letters*, *393*, 2–13. https://doi.org/10.1016/j.epsl.2014.02.037

Ledevin, M., Arndt, N., Chauvel, C., Jaillard, E., & Simionovici, A. (2019). The sedimentary origin of black and white banded cherts of the Buck Reef, Barberton, South Africa. *Geosciences*, *9*, 424. https://doi.org/10.3390/geosciences9100424

Lepot, K. (2020). Signatures of early microbial life from the Archean (4 to 2.5 Ga) eon. *Earth-Science Reviews*, *209*, 103296. https://doi.org/10.1016/j.earscirev.2020.103296

Li, L., Bebout, G. E., & Idleman, B. D. (2007). Nitrogen concentration and $\delta^{15}N$ of altered oceanic crust obtained on ODP legs 129 and 185: Insights into alteration-related nitrogen enrichment and the nitrogen subduction budget. *Geochimica et Cosmochimica Acta*, *71*, 2344–2360. https://doi.org/10.1016/j.gca.2007.02.001

Lowe, D. R., & Worrell, G. F. (1999). Sedimentology, mineralogy, and implications of silicified evaporites in the Kromberg formation, Barberton Greenstone Belt, South Africa. *Special Paper-Geological Society of America*, *329*, 167–188.

Mettam, C., & Zerkle, A. L. (2021). *Nitrogen isotopes in deep time*. Cambridge University Press.

Möbius, J. (2013). Isotope fractionation during nitrogen remineralization (ammonification): Implications for nitrogen isotope biogeochemistry. *Geochimica et Cosmochimica Acta*, *105*, 422–432. https://doi.org/10.1016/j.gca.2012.11.048

Nishizawa, M., Miyazaki, J., Makabe, A., Koba, K., & Takai, K. (2014). Physiological and isotopic characteristics of nitrogen fixation by hyperthermophilic methanogens: Key insights into nitrogen anabolism of the microbial communities in Archean hydrothermal systems. *Geochimica et Cosmochimica Acta*, *138*, 117–135. https://doi.org/10.1016/j.gca.2014.04.021

Nishizawa, M., Sano, Y., Ueno, Y., & Maruyama, S. (2007). Speciation and isotope ratios of nitrogen in fluid inclusions from seafloor hydrothermal deposits at ~3.5 Ga. *Earth and Planetary Science Letters*, *254*, 332–344. https://doi.org/10.1016/j.epsl.2006.11.044

Petrash, D. A., Steenbergen, I. M., Valero, A., Meador, T. B., Pačes, T., & Thomazo, C. (2022). Aqueous system-level processes and prokaryote assemblages in the ferruginous and sulfate-rich bottom waters of a post-mining lake. *Biogeosciences*, *19*, 1723–1751. https://doi.org/10.5194/bg-19-1723-2022

Poulton, S. W., & Canfield, D. E. (2011). Ferruginous conditions: A dominant feature of the ocean through Earth's history. *Elements*, *7*, 107–112. https://doi.org/10.2113/gselements.7.2.107

Raymond, J., Siefert, J. L., Staples, C. R., & Blankenship, R. E. (2004). The natural history of nitrogen fixation. *Molecular Biology and Evolution*, *21*, 541–554. https://doi.org/10.1093/molbev/msh047

Rios-Del Toro, E. E., Valenzuela, E. I., López-Lozano, N. E., Cortés-Martínez, M. G., Sánchez-Rodríguez, M. A., Calvario-Martínez, O., Sánchez-Carrillo, S., & Cervantes, F. J. (2018). Anaerobic ammonium oxidation linked to sulfate and ferric iron reduction fuels nitrogen loss in marine sediments. *Biodegradation*, *29*, 429–442. https://doi.org/10.1007/s10532-018-9839-8

Sebree, J. A., Stern, J. C., Mandt, K. E., Domagal-Goldman, S. D., & Trainer, M. G. (2016). ^{13}C and ^{15}N fractionation of CH_4/N_2 mixtures during photochemical aerosol formation: Relevance to Titan. *Icarus, Titan's Surface and Atmosphere*, *270*, 421–428. https://doi.org/10.1016/j.icarus.2015.04.016

Sigman, D. M., Karsh, K. L., & Casciotti, K. L. (2009). Nitrogen isotopes in the ocean. In J. H. Steele, S. A. Thorpe, & K. K. Turekian (Eds.), *Encyclopedia of ocean sciences* (pp. 40–54). Academic Press. https://doi.org/10.1016/B978-012374473-9.00632-9

Stüeken, E. E., Boocock, T. J., Robinson, A., Mikhail, S., & Johnson, B. W. (2021). Hydrothermal recycling of sedimentary ammonium into oceanic crust and the Archean Ocean at 3.24 Ga. *Geology*, *49*, 822–826. https://doi.org/10.1130/G48844.1

Stüeken, E. E., Buick, R., & Schauer, A. J. (2015). Nitrogen isotope evidence for alkaline lakes on late Archean continents. *Earth and Planetary Science Letters*, *411*, 1–10. https://doi.org/10.1016/j.epsl.2014.11.037

Stüeken, E. E., Kipp, M. A., Koehler, M. C., & Buick, R. (2016). The evolution of Earth's biogeochemical nitrogen cycle. *Earth-Science Reviews*, *160*, 220–239. https://doi.org/10.1016/j.earscirev.2016.07.007

Thomazo, C., Ader, M., & Philippot, P. (2011). Extreme ^{15}N-enrichments in 2.72-Gyr-old sediments: Evidence for a turning point in the nitrogen cycle. *Geobiology*, *9*, 107–120. https://doi.org/10.1111/j.1472-4669.2011.00271.x

Tice, M. M., Bostick, B. C., & Lowe, D. R. (2004). Thermal history of the 3.5–3.2 Ga Onverwacht and fig tree groups, Barberton greenstone belt, South Africa, inferred by Raman microspectroscopy of carbonaceous material. *Geology*, *32*, 37–40. https://doi.org/10.1130/G19915.1

Tice, M. M., & Lowe, D. R. (2004). Photosynthetic microbial mats in the 3,416-Myr-Old ocean. *Nature*, *431*, 549–552. https://doi.org/10.1038/nature02888

Tice, M. M., & Lowe, D. R. (2006a). The origin of carbonaceous matter in pre-3.0 Ga greenstone terrains: A review and new evidence from the 3.42 Ga Buck Reef Chert. *Earth-Science Reviews*, *76*, 259–300. https://doi.org/10.1016/j.earscirev.2006.03.003

Tice, M. M., & Lowe, D. R. (2006b). Hydrogen-based carbon fixation in the earliest known photosynthetic organisms. *Geology*, *34*, 37–40. https://doi.org/10.1130/G22012.1

Tosca, N. J., Jiang, C. Z., Rasmussen, B., & Muhling, J. (2019). Products of the iron cycle on the early earth. *Free Radical Biology and Medicine*, *140*, 138–153. https://doi.org/10.1016/j.freeradbiomed.2019.05.005

Trainer, M. G., Pavlov, A. A., DeWitt, H. L., Jimenez, J. L., McKay, C. P., Toon, O. B., & Tolbert, M. A. (2006). Organic haze on Titan and the early Earth. *PNAS*, *103*, 18035–18042. https://doi.org/10.1073/pnas.0608561103

van Zuilen, M. A., Lepland, A., Teranes, J., Finarelli, J., Wahlen, M., & Arrhenius, G. (2003). Graphite and carbonates in the 3.8 Ga old Isua Supracrustal Belt, southern West Greenland. *Precambrian Research*, *126*, 331–348. https://doi.org/10.1016/S0301-9268(03)00103-7

Ward, B. (2012). The global nitrogen cycle. In A. H. Knoll, D. E. Canfield, & K. O. Konhauser (Eds.), *Fundamentals of geobiology* (pp. 36–48). John Wiley & Sons, Ltd. https://doi.org/10.1002/9781118280874.ch4

Wright, V. P. (2022). The mantle, CO_2 and the giant Aptian chemogenic lacustrine carbonate factory of the South Atlantic: Some carbonates are made, not born. *Sedimentology*, *69*, 47–73. https://doi.org/10.1111/sed.12835

Yamaguchi, K. (2002). *Geochemistry of Archean–Paleoproterozoic black shales: The early evolution of the atmosphere, oceans, and biosphere*. Pennsylvania State University.

Yang, W. H., Weber, K. A., & Silver, W. L. (2012). Nitrogen loss from soil through anaerobic ammonium oxidation coupled to iron reduction. *Nature Geoscience*, *5*, 538–541. https://doi.org/10.1038/ngeo1530

Zerkle, A. L., Claire, M. W., Domagal-Goldman, S. D., Farquhar, J., & Poulton, S. W. (2012). A bistable organic-rich atmosphere on the Neoarchaean Earth. *Nature Geoscience*, *5*, 359–363. https://doi.org/10.1038/ngeo1425

Zhang, X., Sigman, D. M., Morel, F. M. M., & Kraepiel, A. M. L. (2014). Nitrogen isotope fractionation by alternative nitrogenases and past ocean anoxia. *PNAS*, *111*, 4782–4787. https://doi.org/10.1073/pnas.1402976111

Ader, M., Sansjofre, P., Halverson, G. P., Busigny, V., Trindade, R. I. F., Kunzmann, M., & Nogueira, A. C. R. (2014). Ocean redox structure across the late Neoproterozoic oxygenation event: A nitrogen isotope perspective. *Earth and Planetary Science Letters*, *396*, 1–13 10.1016/j.epsl.2014.03.042

SUPPORTING INFORMATION

Additional supporting information can be found online in the Supporting Information section at the end of this article.

How to cite this article: Pellerin, A., Thomazo, C., Ader, M., Marin-Carbonne, J., Alleon, J., Vennin, E., & Hofmann, A. (2023). Iron-mediated anaerobic ammonium oxidation recorded in the early Archean ferruginous ocean. *Geobiology*, *00*, 1–13. https://doi.org/10.1111/gbi.12540